JACS
JOURNAL OF THE AMERICAN CHEMICAL SOCIETY
Article
pubs.acs.org/JACS

Structural Determinants of the Supramolecular Organization of G Protein-Coupled Receptors in Bilayers

Xavier Periole,*[,†] Adam M. Knepp,[‡] Thomas P. Sakmar,[‡] Siewert J. Marrink,[†] and Thomas Huber*[,‡]

[†]Biomolecular Sciences and Biotechnology Institute and Zernike Institute for Advanced Materials, University of Groningen, Nijenborgh 7, 9747AG Groningen, The Netherlands

[‡]Laboratory of Molecular Biology & Biochemistry, The Rockefeller University, 1230 York Avenue, New York, New York 10065, United States

Supporting Information

ABSTRACT: The G protein-coupled receptor (GPCR) rhodopsin self-assembles into supramolecular structures in native bilayers, but the structural determinants of receptor oligomerization are not known. We carried out multiple self-assembly coarse-grained molecular dynamics (CGMD) simulations of model membranes containing up to 64 molecules of the visual receptor rhodopsin over time scales reaching 100 μs. The simulations show strong preferential interaction modes between receptors. Two primary modes of receptor−receptor interactions are consistent with umbrella sampling/potential of mean force (PMF) calculations as a function of the distance between a pair of receptors. The preferential interfaces, involving helices (H) 1/8, 4/5 and 5, present no energy barrier to forming a very stable receptor dimer. Most notably, the PMFs show that the preferred rhodopsin dimer exists in a tail-to-tail conformation, with the interface comprising transmembrane H1/H2 and amphipathic H8 at the extracellular and cytoplasmic surfaces, respectively. This dimer orientation is in line with earlier electron microscopy, X-ray, and cross-linking experiments of rhodopsin and other GPCRs. Less stable interfaces, involving H4 and H6, have a free energy barrier for desolvation (delipidation) of the interfaces and appear to be designed to stabilize "lubricated" (i.e., lipid-coated) dimers. The overall CGMD strategy used here is general and can be applied to study the homo- and heterodimerization of GPCRs and other transmembrane proteins. Systematic extension of the work will deepen our understanding of the forces involved in the membrane organization of integral membrane proteins.

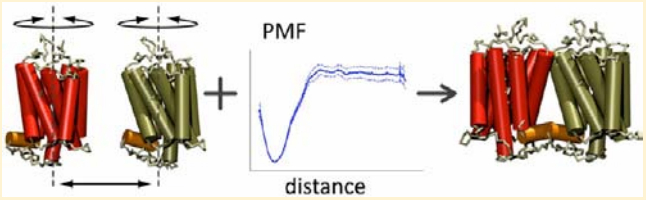

INTRODUCTION

Biological membranes are complex mixtures of various lipids and integral membrane proteins, requiring a precise organization for a proper function. Heptahelical G protein-coupled receptor (GPCRs) form dimers and higher-order oligomers in membranes, although the precise mode and functional consequence of receptor−receptor interaction remains controversial.[1,2] The functional relevance of protein assembly is straightforward in some cases, for instance, the association of multiple subunits to form channels[3] or chemotaxis proteins that cluster to direct the movement of bacterial cells.[4] The functional consequences of oligomerization are known for some GPCRs, e.g., the role of $GABA_B$ receptor subtype heterodimerization in trafficking.[5] But for the majority of rhodopsin-like (class A) GPCRs, including rhodopsin, the functional role of dimerization is not known and is still under active debate.[6] In fact, it has been shown for the visual pigment rhodopsin[7] and the β_2 adrenergic receptor (β_2AR)[8] that a single receptor segregated in membrane nanoparticles is able to activate G proteins. However, mechanisms for how the degree of rhodopsin oligomerization might affect its function have been proposed.[9−11]

Despite these observations from functional reconstitution studies, it has been suggested that highly ordered structural organization could be responsible for the extremely fast electrophysiological response of the phototransduction system.[12] Indeed, atomic force microscopy (AFM) images of native disk membranes adsorbed on a mica surface show structural dimers of rhodopsin organized into rows.[13] Spatial constraints from these AFM images were subsequently used to predict that the primary rhodopsin dimer interface[13] involves transmembrane (TM) helices (H) 4 and 5 (H4/H5 interface). Chemical cross-linking experiments by Javitch and co-workers suggested a similar H4/H5 interface and an alternative H4 interface (excluding H5) in the dopamine D2 receptor (D2R)[14,15] and the δ opioid receptor.[16] This bimodal interface was first interpreted as a possible switch between the two interfaces upon activation[14] and more recently as evidence of higher-order oligomers.[17]

In contrast to those studies emphasizing dimerization around H4 and H5, direct structural evidence has pointed to an interface involving TM H1 and cytoplasmic H8 (H1/H8 interface). In fact, symmetric H1/H8 dimers have previously been observed in two-dimensional (2D)[18] and 3D[19] electron microscopy (EM) and X-ray[20−22] crystallography of opsin,

Received: April 5, 2012
Published: June 8, 2012

   dx.doi.org/10.1021/ja303286e | J. Am. Chem. Soc. 2012, 134, 10959−10965

rhodopsin, and metarhodopsin I and II. Perhaps the most striking demonstration of this interface is the recent crystal structure of the κ-opioid receptor,[23] in which the receptors are organized into dimers nearly identical to those observed in the metarhodopsin-I 3D EM data.[19] The small protein burial of this interface in rhodopsin dimers led some to dismiss the possibility of this dimer as a stable entity in membranes.[24] More recently a similar argument was used to suggest that the μ-opioid receptors interact using an interface involving H5/H6, while the H1/H8 interface was also observed.[25] However, we recently demonstrated close contact between H8 in neighboring rhodopsins in their native ROS membranes. By a combination of cross-linking experiments, partial proteolysis, and high-resolution liquid chromatography−mass spectroscopy (LC−MS), we demonstrated a cross-link between each H8 of the respective protomers in a rhodopsin dimer in native ROS membranes, proving the existence of a symmetric dimer with an H1/H8 interface.[26]

Here we aim to characterize the energetics of receptor−receptor interfaces based on large-scale coarse-grained molecular dynamics (CGMD) simulations. We follow the self-assembly of multiple copies of the receptor over time scales of 10−100 μs, and compute the potentials of mean force (PMFs) of pairs of rhodopsins along specific interfaces. The data clearly show that the most stable dimer conformation displays a symmetrical H1/H8 interface, in agreement with our recent cross-linking experiments[26] and EM density maps.[18,19] The data also point to the existence of weak "lubricated" (i.e., lipid-coated) interfaces, which might stabilize a row-of-dimers supramolecular organization of rhodopsin in disk membranes as seen in AFM images.[13] Overall these results extend our understanding of the biophysical principles underlying lipid−protein interactions and self-assembly processes in membranes.[10,27]

RESULTS

Receptors Self-Assemble into Linear Arrays Stabilized by Preferential Contacts. We previously characterized the effect of the hydrophobic thickness on the self-assembly of rhodopsin dimers and oligomers in systems comprising 16 receptors embedded into a lipid bilayer matrix at 1:100 protein-to-lipid ratio.[27] Here, we extended the length of the simulations and repeated them several times to accumulate a large statistical number of protein−protein contacts. In addition, we explored even bigger membrane patches consisting of 64 receptors at the same protein-to-lipid ratio. In all cases, the membrane consists of $(C20:1)_2PC$ lipids, which, as we have shown previously,[10,27] minimizes the contribution of bilayer deformation (hydrophobic mismatch) to the formation of protein−protein contacts.

Preferential zones of contact between receptors are apparent in the final snapshots (t = 20 μs*) of the multiple self-assembly simulations (Figure 1a). The surfaces of the receptors centered on H8 (site1, Figure 1b; highlighted by a black sphere in Figure 1a,c) and H5 (site3) on the opposite side of rhodopsin are most often involved in a contact. This trend is more evident in the self-assembly simulation of 64 receptors on a 100-μs* time scale (Figure 1c). Primarily based on the same two sites (1 and 3), the receptors form site1−site1, site1−site3, and site3−site3 contacts and assemble into long curvilinear strings, which only marginally interact with each other.

The preferential contact interfaces may also be analyzed by monitoring the relative orientation of the receptors. A set of

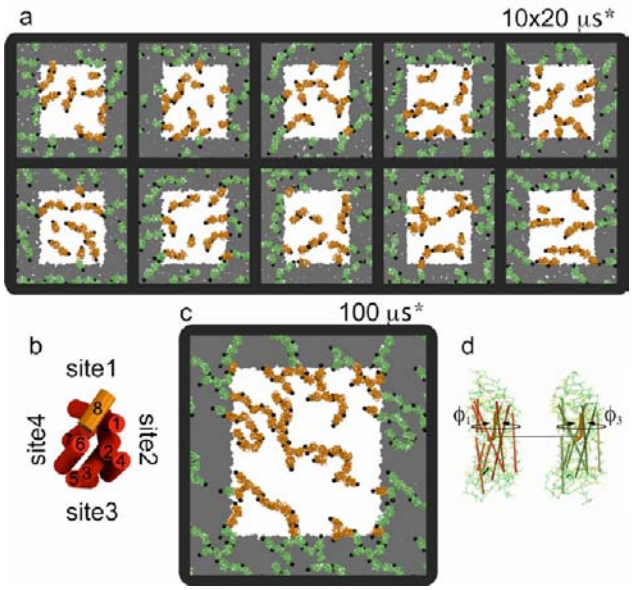

Figure 1. Receptor organization upon self-assembly in 10 independent simulations of 16 receptors (a) and 64 receptors (c). The protein-to-lipid ratio is 1:100. The white area and the orange protein correspond to the unit cell of the simulation box. Black spheres were placed on Cys316 in H8 to ease the visualization of the receptor orientation. (b) A schematic defines the potential sites of interactions of a single rhodopsin as viewed from the cytoplasmic surface. (d) Graphical definition of ϕ_1 and ϕ_3 used in subsequent analysis.

two dihedral angles, ϕ_1 and ϕ_3, can be used to define the orientation of each protein (Figure 1d; cf. Methods and Supporting Information). The dimer conformations may be projected onto a (ϕ_1,ϕ_3) surface, with the buried accessible surface area (ASA), a_b, of the receptor complex used as an additional reaction coordinate to pull out the regions in which the receptors are in contact, i.e., at $a_b > 0$ (Figure 2a). The rather limited number of zones protruding out of the (ϕ_1,ϕ_3) surface despite the large number of contacts formed during the simulations indicates that the receptors interact in a preferential manner.

To discriminate between random contacts and recurrent interfaces, a root-mean-square-difference-based clustering analysis was performed on the rhodopsin dimers collected from the ten trajectories of the 16-rhodopsins self-assembly simulations. Three relative orientations of the receptors predominate (Figure 2b,c and Supporting Information Figure S5). They naturally spot on the three conformations identified above by visual inspection of the end-conformations of the 16-rhodopsins simulations (Figure 1): site1−site1, site1−site3, and site3−site3 arrangements. Notably, the symmetric site1−site1 dimer is defined by a unique and very narrow subspace of (ϕ_1,ϕ_3) (red cluster in Figure 2b) as compared to the other two interfaces, in which multiple closely related variants can be found. On site3 of the receptor, two distinct contact zones could be distinguished: H5 (site3) and H4/H5 (site3′). An alternative interface involving H1 and H8, site1′−site′, was also observed (cluster 286 in Figure 2c). This dimer has a larger buried ASA than the primary site1−site1 arrangement, but it only appeared once in the simulations.

PMFs Reveal Weak and Strong Interfaces. In principle, a PMF can be computed from the corresponding probability distribution function obtained from the spontaneously sampled conformations in *unbiased* simulations.[28,29] Despite the

dx.doi.org/10.1021/ja303286e | J. Am. Chem. Soc. 2012, 134, 10959−10965

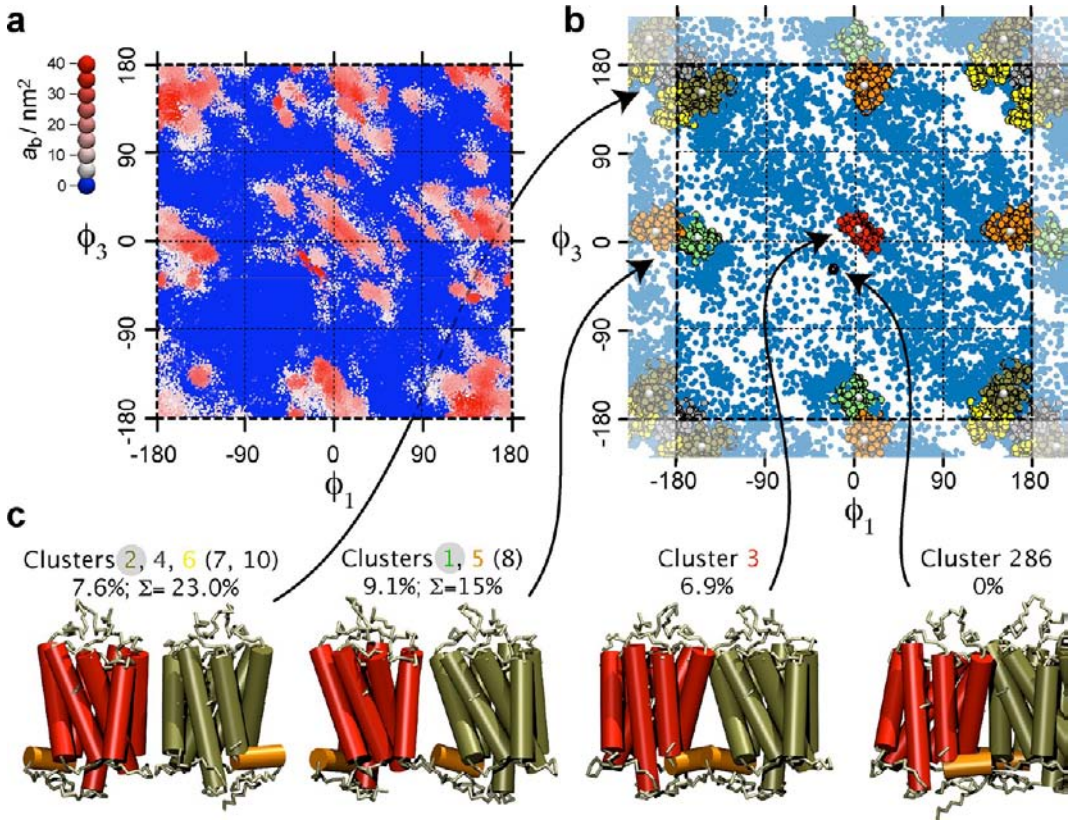

Figure 2. Conformational analysis of the arrangement of receptor dimers formed in self-assembly simulations, and projections of the dimer conformations onto (ϕ_1,ϕ_3) angle space. (a) The dimer conformations are represented by dots colored according to the buried ASA (high a_b, bound dimer; a_b = 0, unbound dimer). The use of a_b as a third dimension and a viewing from the side of the higher a_b emphasizes the (ϕ_1,ϕ_3) subspace primarily explored by the receptor dimers when bound. (b) Subsets of dimer conformations used in the clustering analysis are color-coded according to the cluster to which they belong. The six most populated clusters are highlighted. The blue dots lacking a black rim correspond to dimers from any of the other clusters (7−301). (c) Structures representative of the 10 most populated clusters of the receptor dimers. These 10 clusters are organized into three groups on the basis of the similarity of their relative orientation. (The representative structure of the cluster number 286 is also shown.) When relevant, a gray disk highlights the most populated cluster of the group. For each group the population (%) of the most prominent cluster is given, together with the sum over the entire group.

significant increase of data collected with the self-assembly simulations, there is a clear lack of binding/unbinding events within the time scale simulated. This lack of sampling precludes computation of a meaningful PMF to compare the relative strength of interfaces on a free energy basis. As a complementary approach, we have probed receptor−receptor interfaces by umbrella sampling (US) simulations[30] that enable calculation of PMFs as a function of the distance between pairs of receptors embedded in a solvated membrane bilayer (Figure 3a). A set of weak harmonic restrains (umbrella potentials) was used to control the relative orientation of the receptors and thereby define specific interfaces (inset of Figure 3b). A set of (ϕ_1,ϕ_3) angles was most often sufficient (cf. Methods and Supporting Information). The weighted histogram analysis method (WHAM) is typically used to *unbias* the effect of the *biasing* umbrella potentials.[28,31] We implemented a version of the direct ("histogram-free") formulation of the WHAM algorithm.[31] Our version is generalized for high-dimensional PMFs,[32] and we manually optimized the nested iteration loop structure to obtain an order of magnitude faster computation for high-dimensional PMFs as compared to the original.[33] We compared the interfaces (Figure 3c) formed during the self-assembly simulations, viz., site1−site1, site3−site3, and site3′−site3′, to two other interfaces of the receptors, site2−site2 (H4−H4) and site2−site4 (H4−H6).

The PMFs demonstrate two distinct types of receptor−receptor interacting modes (Figure 3b). In one interacting mode the receptors start feeling each other at $d' \approx 1.2$ nm and smoothly fall into a deep free energy well of 35−55 kJ/mol (8−13 kcal/mol) at a distance at which the receptors are in contact (d' = 0 nm). The distance at which the receptors start seeing each other, d' = 0.9−1.4 nm, and the slope of the free energy profile at short receptor−receptor distances characterize the interfaces falling in that mode. In the second interacting mode, as the receptors approach each other they face an energy barrier for binding of 10−15 kJ/mol (2.4−3.6 kcal/mol) that starts at $d' \approx 1.4$ nm and culminates at d' = 0.7−0.8 nm. Beyond this free energy barrier, the PMFs indicate the presence of a metastable state at $d' \approx 0.5$ nm, corresponding to a situation in which 3−4 lipids are at the interface between the proteins (Figure 4a). This might suggest the existence of lubricated receptor interactions. Past this free energy barrier ($d' \approx 0.25$ nm) the system falls into a shallow free energy well stabilizing the dimer by 5−10 kJ/mol (1.2−2.4 kcal/mol), which is much less than for the first type of interacting modes.

The interfaces that are part of the first type of interacting modes, site1 (H1/H8), site3′ (H4/H5), and site3 (H5), may be referred to as the "strong" interfaces and those of the second type, site2 (H4) and site4 (H6), as the "weak" interfaces. This description of the receptor−receptors interfaces by the PMFs is

dx.doi.org/10.1021/ja303286e | J. Am. Chem. Soc. 2012, 134, 10959−10965

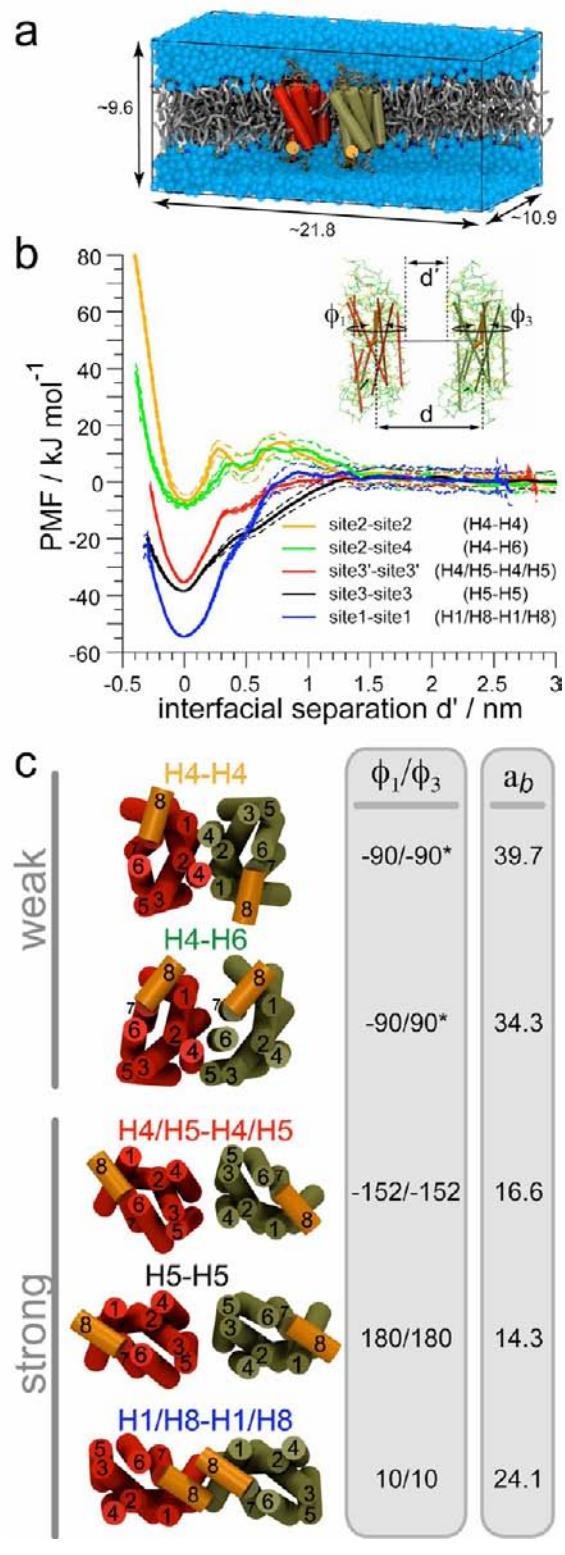

Figure 3. Potentials of mean force of receptor interfaces. (a) Molecular system used to generate the PMFs: two receptors (H8 is orange) embedded in a membrane $(C20:1)_2PC$ bilayer (gray) solvated by water (blue). The lipid and water molecules are only partially shown to feature the receptors. The dimensions of the simulation box are given in nm. The protein-to-lipid ratio was 1:328. (b) PMFs are expressed as a function of the interfacial distance (d'). The set of restraints used to control the distance (d) and the relative orientation (ϕ_1,ϕ_3) of the receptors in shown in the inset. (c) Illustration of the interfaces; a_b is the protein burial (nm^2).

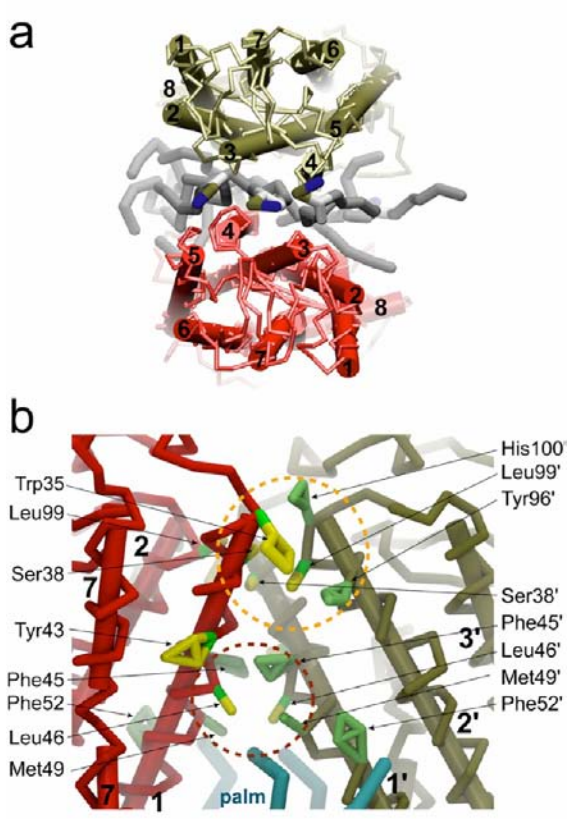

Figure 4. Dimer interaction interface. (a) Interfacial lipids in site2−site2 (weak) dimer. (b) Interacting-residue network in the site1−site1 (strong) dimer. The palmitoyl chains (palm) are shown in cyan stick, an orange dashed line encircles the residues from H1 and H2 involved in the contacts, and in the middle of the bilayer a few interacting residues are shown within an ochre dashed circle. Side chains shown in green were found to be relevant for the dimer in the X-ray packing data.[21,24] Side chains shown in yellow were revealed from the CGMD data: Trp35, Leu99, Ser38, Leu46, and potentially Tyr43 through an interaction with Phe45′.

consistent with the interfaces formed in the self-assembly simulations. The interfaces involving H1/H8, H4/H5, and H5 are predominant in the self-assembly simulations and the interfaces involving H4 and H6 are basically not sampled (Figure 2). This observation faithfully reflects the presence of a free energy barrier to binding in the weak interfaces.

Striking Stability of the Symmetric H1/H8 Interface. Overall, the PMFs show that the symmetric H1/H8 interface is the most stable dimer configuration in our model. It is striking, however, that the protein burial of this interface, although larger than the other two strong interfaces, is significantly smaller than the protein burial of the weak interfaces (Figure 3c). This clearly shows that the strength of a protein−protein interface embedded in a membrane bilayer is not proportional to the associated protein burial, as it is for soluble proteins.[34]

One possible reason for the large stability of the H1/H8−H1/H8 interface is the presence of lipid anchors, notably the palmitoyl chains attached the Cys322 and Cys323 at the end of H8. To test this hypothesis, we performed additional US simulations with a rhodopsin model lacking lipid modifications. The two versions of the PMFs are within the estimated error of ±5 kJ/mol from bootstrap analysis, indicating that the palmitoyl chains do not stabilize the H1/H8 interface. Other functions have been recently suggested for these post-

translational modifications of rhodopsin.[35] Instead, the interface is stabilized by specific residue−residue interactions. Indeed, a well-defined network of interacting residues was found at the receptor−receptor interface on the extracellular side (Figure 4b). A few of these residues (Phe45, Leu46, Met49, Phe52, Tyr96, His100, and the palmitoylated Cys322 and Cys323) have been previously described from the contacts of the H1/H8 dimer found in crystals of rhodopsin.[21,24] In our simulations the proteins adopt a slightly different orientation in the bilayer (Supporting Information Table 1), revealing additional contact residues (Trp35, Ser38, Tyr43, and Leu99 shown in yellow in Figure 4b). Several aromatic and apolar side chains form a strong interacting network on the extracellular side of the bilayer (orange encircled residues in Figure 4b). The strength of this network was apparent from simulations in which the receptors were pulled apart from a configuration in contact to an intermediary distance; the network could hold the two receptors in contact, forcing them to adopt a tilted conformation with the extracellular side still in contact and the cytoplasmic side already separated. It will be interesting to study these interaction networks in the future both by computational and direct experimental methods.

DISCUSSION

Extensive CGMD simulations presented here (covering ∼1.5 ms* in total) suggest that the primary dimer of the visual pigment rhodopsin embedded in a membrane bilayer is a symmetric arrangement interacting through a combination of H1/H2 and H8 at the extracellular and cytoplasmic sides, respectively. We have recently corroborated this computational observation by a set of biochemical cross-linking experiments of rhodopsin in native ROS membranes,[26] where we unambiguously showed the proximity of H8 in each of the respective protomers in a symmetric rhodopsin dimer. The size of the cross-link molecules (2.3−2.6 nm) is compatible with the H1/H8−H1/H8 dimer formed in the self-assembly simulations. An additional configuration was found in these simulations that also matches the cross-linker lengths. Notably, the buried protein surface in this additional binding mode (site1′−site1′) was larger than of the predominant H1/H8−H1/H8 dimer (site1−site1), but this type of dimer was observed only once in the self-assembly simulations.

Symmetric H1/H8 dimers have previously been observed in EM and X-ray crystallography of opsin, rhodopsin, and metarhodopsins I and II.[18−22] Although the relative orientation of the proteins is slightly different in the X-ray structures as compared to the lipid environment we used here, the interfaces represent the same arrangement (Supporting Information Table 2). In contrast, the H1/H8−H1/H8 interface reported for a model of the D2R homodimer based on cross-link experiments[17] shows that the two monomers interact with a different side of H1 (facing H7) as compared with the homodimer of rhodopsin, which uses the side of H1 facing H2. At this point it is not clear if this discrepancy between D2R and rhodopsin is functionally relevant, or if it results from a limitation of the resolution of models built from cross-link experiments. An H1/H8 dimer was also reported for β_2AR based on cross-link[36] and X-ray[37] experiments that show a similar orientation of H1 to what we see in rhodopsin but with an interaction with H8 on the other face of the helix.[37] An H1/H8 interaction following the rhodopsin interface was recently found in the κ-opioid and μ-opioid receptors.[23,25] Taken together this strongly suggests that our model of the H1/H8 symmetric dimer might extend to many other class A GPCRs.

In spite of the early direct structural evidence pointing to the H1/H8 interface,[18,19,21] its relatively small associated protein burial raised doubts about its physiological relevance for rhodopsin[24] and μ-opioid receptors.[25] However, our simulations demonstrate the significance of this interface in addition to others centered on H5. Surprisingly, this protein burial is much less than the one observed for the weak interfaces (H4 and H6), which challenges the potential utility of buried accessible surface area (ASA) as a predictor of the strength of membrane-embedded protein−protein interfaces.[24,25] It is likely and reasonable that different forces must govern protein−protein interactions depending on whether the complex is embedded in a membrane bilayer or in an aqueous environment. In that respect, specific interactions such as those found in the network of residues in contact at the extracellular side of H1 and H2 in the H1/H8 interface (Figure 4a), and lipid−protein interactions in lubricated interfaces as found in the H4−H4 interface (Figure 4b) are pertinent features. These contacts add to the contribution of heterogeneous lipid bilayer deformations at the surface of the protein in response to local hydrophobic mismatch.[27] The lipid composition of the membrane is also a factor of considerable importance, which we intend to address in future work.[10,38,39]

Two very distinct types of receptor−receptor interfaces emerged from our computational modeling: (i) a weak dimer with an energy barrier for binding, and (ii) a strong dimer without an energy barrier for binding (Figure 3). A similar range of variations of protein−protein interactions was reported based on more generic model systems in which the protein and lipid models were modified to probe different situations.[39,40] The protein primary structure may encode for the presence of such heterogeneous surfaces on a single protein and thereby yield to predefined protein−protein contacts. In the case of rhodopsin the presence of weak and strong interfaces naturally leads to the supramolecular organization shown in Figure 5. The model follows the structural information obtained from the AFM images showing rows of dimers interacting through a strong interface (H1/H8) and stabilized by lubricated weak protein contacts. This supramolecular arrangement was stable over a μs* time scale.

CONCLUSION

The combined CGMD self-assembly simulations and PMFs of rhodopsin provide new biophysical insights on the complex interplay of forces that guide protein−protein interactions in membrane bilayers. Different modes of interactions between receptor−receptor interfaces determine higher-order organization. The primary dimer in rhodopsin oligomers is a tail-to-tail configuration with significant interaction between TM H1/H2 at the extracellular surface and amphipathic cytoplasmic H8. Other interaction interfaces involve H4, H5, and H6 to facilitate the possibility of higher-order structure. Given the overall similarities in the helical arrangement and membrane topology of GPCRs, these results suggest a common mechanism for receptor homo- and hetero-oligomerization and potentially a model of the supramolecular structure of the GPCR signalosome.

METHODS

Computational Methods. The long-time-scale and large-system simulations were performed using the MARTINI force field[41] and its

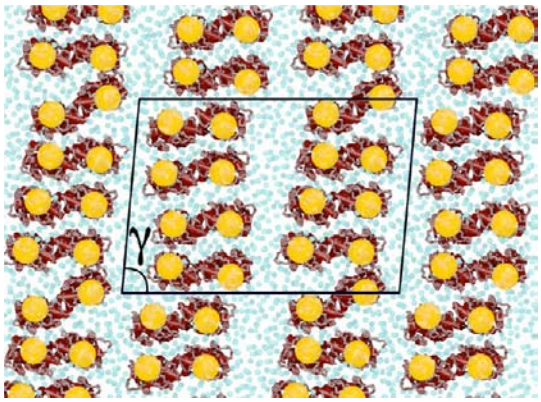

Figure 5. Model of the rows-of-dimers organization of rhodopsin molecules after a 16-μs* CGMD simulation. The starting conformation was built according to the cell dimensions determined from AFM images of rhodopsin in disk membranes prepared from mouse retinas[13,49] (Supporting Information Figure S3). The lipid molecules are shown as cyan dots placed at the location of the phosphate groups. Rhodopsins are shown in deep red using cylinders for the helices and gray tubes for the backbone trace. The large orange spheres are centered on Thr242 to show the H6 protrusion. The monoclinic unit cell (γ = 85°) is outlined by a black box; the view is from the cytoplasmic surface. Note that the protein-to-lipid ratio is 1:36, about twice as large as in bovine ROS disk membranes with 1:70 (see Methods for details).

extension to proteins.[42] An elastic network has been used to maintain the structure of individual proteins while preserving their internal flexibility.[43] The US technique was used to determine the PMFs that quantify the strength of receptor−receptor interactions as interfaces and distances between a pair of receptors were varied. The relative orientation of receptors in the dimer pairs was controlled by the use of soft harmonic potentials (virtual bond algorithm[44]). The relative strength of the interfaces may be compared because these additional restraints were also included in the unbiasing procedure, a six-dimensional extension of the weighted histogram analysis method (WHAM).[31,33] A total of 1.174 ms* of simulation time was used to explore the five interfaces probed (see Supporting Information for more details). The use of an effective time to account for the speed up (factor four for lipids and membrane proteins[27,45]) of our coarse-grain model is indicated by an *. The H1/H8−H1/H8 rhodopsin dimer (Figure 1) is virtually identical to one we built by rigid-body fitting of the PDB:1GZM rhodopsin structure to the cryo-EM density map (EMDataBank entry EMD-1079[19]) using the Situs2.5 package[46] (Supporting Information Table 1). The self-assembly and PMF simulations used protein-to-lipid ratios of 1:100 and 1:328, respectively.

Supramolecular Structure Analysis. We modeled a hypothetical supramolecular structure of the ROS disk membrane that was consistent with the H1/H8−H1/H8 rhodopsin dimer and the rows-of-dimers observed by AFM imaging.[13] The rows-of-dimers pattern of rhodopsin is generally consistent with negatively stained EM images of outer segment membranes,[47] small-angle X-ray scattering of magnetically oriented ROS membranes,[48] cryo-EM 2D and 3D crystallography,[18,19] and AFM imaging.[13] Visual inspection of the published AFM images indicates some variability of the rows-of-dimers arrangement, and the row-to-row spacing also varied significantly in the images, but the closest spacing in paracrystalline regions was noted to be 8.4 nm, which is comparable to the distance of 8.3 nm found in 2D crystals[18] with similar overall organization. The spacing between dimers in a row is generally about 3.8 nm in the AFM images, which is only slightly larger than the 3.2 nm found in the 2D crystals.[18] Our model suggests a row-to-row spacing of 10.89 nm, consistent with the average packing density of 48 300 rhodopsin/μm^2 as found in the AFM studies.[13,49] The increase in distance could be explained by the larger phospholipid-to-protein ratio as compared to the 2D crystal. The corresponding area is 20.70 nm^2 per lipid-solvated rhodopsin in the disk membrane. Together with the 9.0 nm^2 area of rhodopsin in the bilayer,[50] this packing density leaves space for ∼36 phospholipids per rhodopsin (at 0.65 nm^2 per lipid[29]), which is about half of the value determined for bovine rod outer segment disk membranes.[51,52] It is unclear why the average rhodopsin packing density in disk membranes from mice[13,49,53] is approximately twice as large as compared to previous estimates.[54,55] Note that an extension of the row-to-row distance from 10.89 to 15.28 nm in our model would lead to a protein-to-lipid ratio of 1:60. In this respect, it is noteworthy that the rhodopsin interaction mode in our model is also consistent with the packing from EM crystallography of rhodopsin,[18] which differs from the earlier interpretation of the AFM data.[49] Details of the models and simulation protocols are published as Supporting Information.

Limitations of the Model and Methodology. It is important to point out some of the limitations underlying our model and the methodology used. First, the processes studied involve the slow diffusion of lipid and protein, which led to difficulty reaching complete convergence on some aspects of the data presented. Notably in the self-assembly simulations the lack of protein binding/unbinding events limited the spontaneous self-assembly simulations to only reflect the long- and medium-range interactions depicted by the PMFs. The interfaces having an energy barrier to binding are poorly sampled and the populations of the ones sampled do not reflect relative stabilities. In the PMFs the slow exchange of interfacial lipids with the bulk lipids, alternatively, makes both a full lipidation and delipidation of some interfaces extremely challenging to sample at equilibrium even on time scales up to 20 μs* per window. Equilibrium sampling is critical to obtain reliable PMFs. Note also that the restriction of the PMFs to slices of the hyper-surface (of the relative protein orientation) significantly reduced the need of conformational sampling. We have shown previously that for a single transmembrane helix protein, glycophorin A (GpA), embedded in a membrane bilayer it takes up to 8 μs* to sufficiently sample the rotational degree of freedom to reach convergence for umbrella windows where the peptides are in contact.[56] Therefore, the quantitative details of the PMFs presented in the manuscript have to be considered with care, but the qualitative features are consistent and significant. A second limitation may be the use of a CG model describing the protein−protein interactions. It has been observed that in an aqueous environment CG protein−protein interactions might be slightly overstabilized but there is no similar evidence for membrane proteins. In fact we have recently reported studies of the association of GpA[56] and WALP peptides[38] in model membranes using the same MARTINI CG model and found that the free energy profile of the GpA peptide was essentially identical to one reported earlier using an atomistic force field[57] and that the estimated dimerization free energy of the WALP peptides agreed with the value obtained from fluorescence resonance energy transfer experiments.[58] The rotational and translational diffusion of rhodopsin was also found to be in close agreement with experiments.[27] It is also important to note that individual side chain−side chain association constants are overall in relatively good agreement with their atomistic homologues.[59]

■ ASSOCIATED CONTENT

Ⓢ Supporting Information

Detailed descriptions of the CGMD technique, simulations performed, method used to determine the PMF, and analyses. This material is available free of charge via the Internet at http://pubs.acs.org.

■ AUTHOR INFORMATION

Corresponding Author

x.periole@rug.nl; hubert@rockefeller.edu

Notes

The authors declare no competing financial interest.

■ ACKNOWLEDGMENTS

This work was supported by The Netherlands Organisation for Scientific Research (NWO) (X.P and S.J.M., ECHO.08.BM.041), the Allene Reus Memorial Trust, the Crowley Family Fund, the Danica Foundation, and NIH R01 EY012049 (A.M.K., T.H., and T.P.S.). Computer time was allocated by The Netherlands National Computing Facilities Foundation (NCF grant SH-113-V-08).

■ REFERENCES

(1) Pin, J. P.; Neubig, R.; Bouvier, M.; Devi, L.; Filizola, M.; Javitch, J. A.; Lohse, M. J.; Milligan, G.; Palczewski, K.; Parmentier, M.; Spedding, M. *Pharmacol. Rev.* **2007**, *59*, 5.
(2) Palczewski, K. *Trends Biochem. Sci.* **2010**, *35*, 595.
(3) Doyle, D. A.; Cabral, J. M.; Pfuetzner, R. A.; Kuo, A. L.; Gulbis, J. M.; Cohen, S. L.; Chait, B. T.; MacKinnon, R. *Science* **1998**, *280*, 69.
(4) Adler, J. *Annu. Rev. Biochem.* **1975**, *44*, 341.
(5) White, J. H.; Wise, A.; Main, M. J.; Green, A.; Fraser, N. J.; Disney, G. H.; Barnes, A. A.; Emson, P.; Foord, S. M.; Marshall, F. H. *Nature* **1998**, *396*, 679.
(6) Chabre, M.; Cone, R.; Saibil, H. *Nature* **2003**, *426*, 30.
(7) Banerjee, S.; Huber, T.; Sakmar, T. P. *J. Mol. Biol.* **2008**, *377*, 1067.
(8) Whorton, M. R.; Bokoch, M. P.; Rasmussen, S. G. F.; Huang, B.; Zare, R. N.; Kobilka, B.; Sunahara, R. K. *Proc. Natl. Acad. Sci. U.S.A.* **2007**, *104*, 7682.
(9) Niu, S. L.; Mitchell, D. C. *Biophys. J.* **2005**, *89*, 1833.
(10) Botelho, A. V.; Huber, T.; Sakmar, T. P.; Brown, M. F. *Biophys. J.* **2006**, *91*, 4464.
(11) Soubias, O.; Gawrisch, K. *Biochim. Biophys. Acta-Biomembranes* **2012**, *1818*, 234.
(12) Dell'Orco, D.; Schmidt, H. *J. Phys. Chem. B* **2008**, *112*, 4419.
(13) Fotiadis, D.; Liang, Y.; Filipek, S.; Saperstein, D. A.; Engel, A.; Palczewski, K. *Nature* **2003**, *421*, 127.
(14) Guo, W.; Shi, L.; Filizola, M.; Weinstein, H.; Javitch, J. A. *Proc. Natl. Acad. Sci. U.S.A.* **2005**, *102*, 17495.
(15) Guo, W.; Shi, L.; Javitch, J. A. *J. Biol. Chem.* **2003**, *278*, 4385.
(16) Johnston, J. M.; Aburi, M.; Provasi, D.; Bortolato, A.; Urizar, E.; Lambert, N. A.; Javitch, J. A.; Filizola, M. *Biochemistry* **2011**, *50*, 1682.
(17) Guo, W.; Urizar, E.; Kralikova, M.; Mobarec, J. C.; Shi, L.; Filizola, M.; Javitch, J. A. *EMBO J.* **2008**, *27*, 2293.
(18) Schertler, G. F. X.; Hargrave, P. A. *Proc. Natl. Acad. Sci. U.S.A.* **1995**, *92*, 11578.
(19) Ruprecht, J. J.; Mielke, T.; Vogel, R.; Villa, C.; Schertler, G. F. X. *EMBO J.* **2004**, *23*, 3609.
(20) Park, J. H.; Scheerer, P.; Hofmann, K. P.; Choe, H. W.; Ernst, O. P. *Nature* **2008**, *454*, 183.
(21) Salom, D.; Lodowski, D. T.; Stenkamp, R. E.; Le Trong, I.; Golczak, M.; Jastrzebska, B.; Harris, T.; Ballesteros, J. A.; Palczewski, K. *Proc. Natl. Acad. Sci. U.S.A.* **2006**, *103*, 16123.
(22) Choe, H. W.; Kim, Y. J.; Park, J. H.; Morizumi, T.; Pai, E. F.; Krauss, N.; Hofmann, K. P.; Scheerer, P.; Ernst, O. P. *Nature* **2011**, *471*, 651.
(23) Wu, H.; Wacker, D.; Mileni, M.; Katritch, V.; Han, G. W.; Vardy, E.; Liu, W.; Thompson, A. A.; Huang, X. P.; Carroll, F. I.; Mascarella, S. W.; Westkaemper, R. B.; Mosier, P. D.; Roth, B. L.; Cherezov, V.; Stevens, R. C. *Nature* **2012**, *485*, 327.
(24) Lodowski, D. T.; Salom, D.; Le Trong, I.; Teller, D. C.; Ballesteros, J. A.; Palczewski, K.; Stenkamp, R. E. *J. Struct. Biol.* **2007**, *158*, 455.
(25) Manglik, A.; Kruse, A. C.; Kobilka, T. S.; Thian, F. S.; Mathiesen, J. M.; Sunahara, R. K.; Pardo, L.; Weis, W. I.; Kobilka, B. K.; Granier, S. *Nature* **2012**, *485*, 321.
(26) Knepp, A. M.; Periole, X.; Marrink, S. J.; Sakmar, T. P.; Huber, T. *Biochemistry* **2012**, *51*, 1819.
(27) Periole, X.; Huber, T.; Marrink, S. J.; Sakmar, T. P. *J. Am. Chem. Soc.* **2007**, *129*, 10126.
(28) Roux, B. *Comput. Phys. Commun.* **1995**, *91*, 275.
(29) Huber, T.; Rajamoorthi, K.; Kurze, V. F.; Beyer, K.; Brown, M. F. *J. Am. Chem. Soc.* **2002**, *124*, 298.
(30) Torrie, G. M.; Valleau, J. P. *J. Comput. Phys.* **1977**, *23*, 187.
(31) Kumar, S.; Bouzida, D.; Swendsen, R. H.; Kollman, P. A.; Rosenberg, J. M. *J. Comput. Chem.* **1992**, *13*, 1011.
(32) Kumar, S.; Rosenberg, J. M.; Bouzida, D.; Swendsen, R. H.; Kollman, P. A. *J. Comput. Chem.* **1995**, *16*, 1339.
(33) Souaille, M.; Roux, B. *Comput. Phys. Commun.* **2001**, *135*, 40.
(34) Chothia, C.; Janin, J. *Nature* **1975**, *256*, 705.
(35) Olausson, B. E.; Grossfield, A.; Pitman, M. C.; Brown, M. F.; Feller, S. E.; Vogel, A. *J. Am. Chem. Soc.* **2012**, *134*, 4324.
(36) Fung, J. J.; Deupi, X.; Pardo, L.; Yao, X. J.; Velez-Ruiz, G. A.; DeVree, B. T.; Sunahara, R. K.; Kobilka, B. K. *EMBO J.* **2009**, *28*, 3315.
(37) Cherezov, V.; Rosenbaum, D. M.; Hanson, M. A.; Rasmussen, S. G. F.; Thian, F. S.; Kobilka, T. S.; Choi, H. J.; Kuhn, P.; Weis, W. I.; Kobilka, B. K.; Stevens, R. C. *Science* **2007**, *318*, 1258.
(38) Schafer, L. V.; de Jong, D. H.; Holt, A.; Rzepiela, A. J.; de Vries, A. H.; Poolman, B.; Killian, J. A.; Marrink, S. J. *Proc. Natl. Acad. Sci. U.S.A.* **2011**, *108*, 1343.
(39) de Meyer, F. J. M.; Rodgers, J. M.; Willems, T. F.; Smit, B. *Biophys. J.* **2010**, *99*, 3629.
(40) de Meyer, F. J. M.; Venturoli, M.; Smit, B. *Biophys. J.* **2008**, *95*, 1851.
(41) Marrink, S. J.; Risselada, H. J.; Yefimov, S.; Tieleman, D. P.; de Vries, A. H. *J. Phys. Chem. B* **2007**, *111*, 7812.
(42) Monticelli, L.; Kandasamy, S. K.; Periole, X.; Larson, R. G.; Tieleman, D. P.; Marrink, S. J. *J. Chem. Theory Comput.* **2008**, *4*, 819.
(43) Periole, X.; Cavalli, M.; Marrink, S. J.; Ceruso, M. A. *J. Chem. Theory Comput.* **2009**, *5*, 2531.
(44) Boresch, S.; Tettinger, F.; Leitgeb, M.; Karplus, M. *J. Phys. Chem. B* **2003**, *107*, 9535.
(45) Ramadurai, S.; Holt, A.; Schafer, L. V.; Krasnikov, V. V.; Rijkers, D. T. S.; Marrink, S. J.; Killian, J. A.; Poolman, B. *Biophys. J.* **2010**, *99*, 1447.
(46) Wriggers, W.; Milligan, R. A.; McCammon, J. A. *J. Struct. Biol.* **1999**, *125*, 185.
(47) Blasie, J. K.; Dewey, M. M.; Blaurock, A. E.; Worthington, C. R. *J. Mol. Biol.* **1965**, *14*, 143.
(48) Chabre, M. *Biochim. Biophys. Acta* **1975**, *382*, 322.
(49) Liang, Y.; Fotiadis, D.; Filipek, S.; Saperstein, D. A.; Palczewski, K.; Engel, A. *J. Biol. Chem.* **2003**, *278*, 21655.
(50) Huber, T.; Botelho, A. V.; Beyer, K.; Brown, M. F. *Biophys. J.* **2004**, *84*, 2078.
(51) Stone, W. L.; Farnsworth, C. C.; Dratz, E. A. *Exp. Eye Res.* **1979**, *28*, 387.
(52) Wiedmann, T. S.; Pates, R. D.; Beach, J. M.; Salmon, A.; Brown, M. F. *Biochemistry* **1988**, *27*, 6469.
(53) Liang, Y.; Fotiadis, D.; Maeda, T.; Maeda, A.; Modzelewska, A.; Filipek, S.; Saperstein, D. A.; Engel, A.; Palczewski, K. *J. Biol. Chem.* **2004**, *279*, 48189.
(54) Liebman, P. A.; Entine, G. *Science* **1974**, *185*, 457.
(55) Pugh, E. N.; Lamb, T. D. *Biochim. Biophys. Acta* **1993**, *1141*, 111.
(56) Sengupta, D.; Marrink, S. J. *Phys. Chem. Chem. Phys.* **2010**, *12*, 12987.
(57) Henin, J.; Pohorille, A.; Chipot, C. *J. Am. Chem. Soc.* **2005**, *127*, 8478.
(58) Yano, Y.; Matsuzaki, K. *Biochemistry* **2006**, *45*, 3370.
(59) de Jong, D. H.; Periole, X.; Marrink, S. J. *J Chem Theory Comput* **2012**, in press.